Impact of unmitigated HFC emissions on stratospheric ozone at the end of the 21$^{\text{st}}$ century as simulated by chemistry-climate models

E. Dupuy[1], H. Akiyoshi[1], Y. Yamashita[2,1]

[1]National Institute for Environmental Studies (NIES), 16-2 Onogawa, 305-8506 Tsukuba, Japan

[2]Japan Agency for Marine-Earth Science and Technology (JAMSTEC), 3173-25 Showa-machi,

Kanazawa-ku, 236-0001 Yokohama, Japan

Key Points:

- Unregulated HFCs have a small, global impact on total ozone by the end of the century.
- HFCs cause altitude-dependent positive and negative ozone changes at low and mid-latitudes.
- Wave activity in the wintertime polar stratosphere induces large differences in ozone response to an HFC increase between the models.

Corresponding author: Hideharu Akiyoshi, `hakiyosi@nies.go.jp`

Abstract

Hydrofluorocarbons (HFCs) have been increasingly replacing chlorofluorocarbons and hydrochlorofluorocarbons. Although their ozone-depleting potential is negligible, as potent greenhouse gases they indirectly influence stratospheric ozone recovery. Measurements and model projections must continue to evaluate HFC limitation measures and assess the long-term impact of HFCs on the atmospheric radiation budget and stratospheric ozone. In this study, we present multi-member ensemble simulations designed to estimate the impact of HFCs on stratospheric temperature, ozone and circulation changes at the end of the century. We compared simulations with and without HFCs for two three-dimensional chemistry-climate models that use the same chemistry module but different physical schemes. At low and mid-latitudes, temperature and ozone responses were comparable for both models and in general agreement with previous studies. HFCs induced a marked temperature increase up to 5 hPa and vertically alternating positive and negative ozone anomalies. We explained this pattern by competing effects of vertical motion (low and middle stratosphere) and temperature (upper stratosphere) anomalies. At northern high latitudes, there were strong discrepancies with previous studies and between the models themselves, attributed to differences in ozone anomalies caused by wave activity during winter. Quantitatively, we found a net positive, but small, HFC impact on total ozone amounts. Largest anomalies were less than 1% in the winter polar stratosphere. Our results indicate that increasing HFC amounts will likely have a limited impact on stratospheric ozone recovery within this century, with large uncertainty in the polar regions.

1 Introduction

Chlorofluorocarbons (CFCs) and their transitional replacements, the hydrochlorofluorocarbons (HCFCs), are major contributors to stratospheric ozone (O_3) depletion through chlorine- and bromine-induced catalytic cycles. Following successful implementation of the 1987 Montreal Protocol and its successive amendments and adjustments, atmospheric amounts of ozone-depleting substances (ODSs, including CFCs and HCFCs) have measurably decreased (WMO, 2018). As a consequence, stratospheric ozone levels have begun recovering. They are expected to return to 1980 values between 2030 and 2060, depending on the latitude (Amos et al., 2020; Dhomse et al., 2018; Bednarz et al., 2016).

Hydrofluorocarbons (HFCs) are purely anthropogenic compounds that were developed as substitutes of both CFCs and HCFCs. They have become progressively dominant in diverse applications, such as air conditioning, refrigeration or thermal insulation (UNEP, 2011). Subsequently, their atmospheric concentrations have increased rapidly since the early 1990s (WMO, 2014). Because they do not contain chlorine or bromine atoms, HFCs do not contribute to the chlorine- or bromine-induced catalytic cycles that lead to stratospheric O_3 destruction. Therefore, their ozone-depleting potentials (ODPs) are negligible (WMO, 2018). Most HFCs currently used have long stratospheric lifetimes, because they do not absorb stratospheric ultraviolet (UV) radiation (SPARC, 2013). Their main removal process is reaction with the hydroxyl radical (OH) in the troposphere (WMO, 2018). Due to these long lifetimes and to strong infrared (IR) absorption in the atmospheric window (8–14 µm), many HFCs are potent greenhouse gases (GHGs) (WMO, 2014). Therefore, they substantially affect stratospheric temperature and circulation patterns. This, in turn, influences the concentration and variations of stratospheric O_3.

Due to their role in climate change, steps were taken to curb the production and use of HFCs. The Kigali Amendment to the Montreal Protocol was ratified in 2016 and came into force in 2019. Although uncertainties remain on future HFC release from long-term banks (e.g., refrigerators or insulation, Velders et al., 2009), full compliance with the Kigali amendment should ensure that HFC emissions will peak around 2040 (WMO, 2018; Velders et al., 2014). Until then, however, their atmospheric abundance will keep increasing. Therefore, to evaluate the future impact of HFCs on the atmospheric radiation budget and verify that all parties comply with their pledges under the Kigali Amendment, measurements and model projections must continue.

The only HFC measurements with near-global coverage currently available have been performed since 2004 by the Atmospheric Chemistry Experiment–Fourier Transform Interferometer (ACE-FTS, Bernath et al., 2005). Global distribution estimates of fluorine compounds, including HFC-23 and HFC-134a, have been retrieved from the upper troposphere to the mid-stratosphere (7–25 km) from the ACE-FTS data (Fernando et al., 2019; Nassar et al., 2006). Other measurements of HFCs are available from ground-based observation networks, such as the Advanced Global Atmospheric Gases Experiment (AGAGE) (e.g., Simmonds et al., 2017) or the National Oceanic and Atmospheric Administration (NOAA) (e.g., Montzka et al., 2015) networks. Although these include only a limited number of stations, they each have been operating for decades and their

importance for climate change monitoring is established. For instance, measurements from these networks were used to confirm the transition from CFCs / HCFCs to HFCs and to observe the increase of HFC abundances, including deviations from the expected trends (e.g, Stanley et al., 2020; Montzka et al., 2018; Simmonds et al., 2017; Lunt et al., 2015).

In order to assess the potential impact of HFCs on stratospheric ozone recovery, their future contribution to atmospheric radiative changes must be evaluated using climate model simulations. Forster and Joshi (2005) performed Fixed Dynamical Heating simulations and showed that, similarly to ODSs, a halocarbon concentration increase induces a net temperature increase in the stratosphere and in the troposphere. This is different from the radiative effect of carbon dioxide (CO_2), for which increasing concentrations induce global tropospheric warming and stratospheric cooling (Forster & Joshi, 2005). The impact of HFCs on temperature and O_3 was simulated by Hurwitz et al. (2015) using a two-dimensional model. Like Forster and Joshi (2005) for halocarbons, they found that HFCs caused an altitude-dependent heating of the troposphere and the stratosphere, with a temperature response increasing from the troposphere to the mid-stratosphere (with a maximum around 70 hPa near the Equator), then decreasing to near-zero in the uppermost stratosphere. They found largest ozone response changes in the tropics, with increasingly positive O_3 concentration changes from the troposphere up to 70–80 hPa, then negative values from a strong minimum in the middle stratosphere to slightly negative, near-zero differences in the uppermost stratosphere. In the polar regions, O_3 variations were smaller but similar: positive up to the lower stratosphere and negative above, with largest values in the middle stratosphere. Their simulations also showed a strengthening of the stratospheric mean meridional (Brewer-Dobson) circulation above 18 km, with increased upward motion at low latitudes and increased downward motion at mid- and polar latitudes (Hurwitz et al., 2015). Below 18 km in the tropics and sub-tropics, the mean (Hadley) circulation became weaker. Integrating over the atmospheric column, Hurwitz et al. (2015) found that HFCs caused a net, but weak, global decrease of total ozone. Finally, they established that HFC effects are linear and scalable to their atmospheric abundance (Hurwitz et al., 2015).

In this work, we present the first results of three-dimensional, multi-member ensemble simulations designed to evaluate the impact of increasing HFC concentrations on stratospheric ozone and temperature. We perform the same simulations for two chemistry-climate models (CCMs). These models share the same chemistry module, but parts of

113 their physical schemes are different, thus the models differ in the way they simulate cli-

114 mate phenomena. We analyze the HFC-induced effects in terms of temperature, ozone

115 and circulation changes, and estimate the statistical relevance of our results.

2 Methodology

2.1 Chemistry-Climate Models Used in this Study

118 For our analyses, we use two CCMs based on different versions of a coupled atmosphere-

119 ocean general circulation model, the Model for Interdisciplinary Research on Climate (MIROC).

120 The earlier version, MIROC3.2, was developed jointly at the Center for Climate System

121 Research (CCSR), the National Institute of Environmental Studies (NIES) and the Fron-

122 tier Research Center for Global Change (FRCGC) (K1 model developers, 2004; Numaguti

123 et al., 1997). The newer version, MIROC5, is a joint effort of CCSR, NIES and the Japan

124 Agency for Marine-Earth Science and Technology (JAMSTEC) (Watanabe et al., 2010).

125 The atmospheric components of both models have the same dynamical core. However,

126 there were several updates or replacements of physical processes in MIROC5 to account

127 for known MIROC3.2 limitations. For example, some studies found deficiencies in the

128 reproduction of natural variability by MIROC3.2. Cloud representation was also signif-

129 icantly refined from MIROC3.2 to MIROC5 to improve climate sensitivity (Watanabe

130 et al., 2010, and references therein). Other differences between the two versions have been

131 extensively documented by Watanabe et al. (2010) and will not be repeated here.

132 The models used for our study are based on MIROC3.2 and MIROC5 and desig-

133 nated hereafter as MIROC3.2-CCM and MIROC5-CCM, respectively. Both are spectral

134 models and use a flux-form semi-Lagrangian advection scheme for transport of chemi-

135 cal constituents. The horizontal resolution is T42 ($2.8° \times 2.8°$). The vertical coordinate

136 is a hybrid sigma-pressure coordinate, with 34 vertical layers from the surface to about

137 0.003 hPa ($\sim$80 km). Both versions include a radiative transfer scheme with 32 spectral

138 bins, in the "solar" spectral range at UV/visible and near-IR wavelengths (200–690 nm

139 for species relevant to ozone chemistry, and 690 nm to 4 μm, respectively), and at longer

140 wavelengths relevant to terrestrial IR radiation (4–1000 μm). The CCMs are not cou-

141 pled to the ocean module of MIROC. Instead, sea surface temperature (SST) and sea

142 ice are fixed to the settings used for the fifth assessment report of the Intergovernmen-

143 tal Panel on Climate Change (IPCC-AR5) (Morgenstern et al., 2017; IPCC, 2014).

144   Both models use the same dedicated stratospheric chemistry module, developed by

145   NIES and CCSR. It includes 61 chemical constituents, and 165 gas-phase and 42 pho-

146   tolytic reactions (Akiyoshi et al., 2016). Heterogeneous chemistry is simulated by 13 re-

147   actions, with multiple types of aerosol – water (H_2O), sulfate (H_2SO_4), nitric acid (HNO_3)

148   – explicitly considered. Polar stratospheric clouds of type 1 (nitric acid trihydrate or NAT),

149   2 (ice) and supercooled ternary solutions (STS) are included (Morgenstern et al., 2017;

150   Akiyoshi et al., 2016).

2.2 Multi-Member Ensemble Simulations for HFCs

152   In order to obtain some statistical assessment of the impact of HFCs on stratospheric

153   ozone, we perform a set of multi-member ensemble simulations, in identical conditions,

154   for both MIROC3.2-CCM and MIROC5-CCM. The HFC-dedicated simulations (here-

155   after "experiments") differ only by the initial amount of HFCs. For all experiments, the

156   background atmosphere is initialized to projected conditions in 2095. GHG abundances

157   are set to their 2095 value in the Representative Concentration Pathway (RCP) 2.6 sce-

158   nario (stringent mitigation) established for IPCC-AR5 (IPCC, 2014). In this scenario,

159   CO_2 concentrations are expected to peak around 2040, then to stabilize and start de-

160   creasing before the end of the century. ODS abundances are set to their 2095 values in

161   scenario A1 of the World Meteorological Organization (WMO-A1) (WMO, 2014). All

162   experiments assume full compliance with the Montreal Protocol and its amendments.

163   We devise three experimental settings (Table 1) that are used for both models. For

164   each setting, we assign constant global abundances to four main HFC compounds: HFC-

165   125, HFC-143a, HFC-32 and HFC-134a. Another compound, HFC-23, has a very long

166   atmospheric lifetime, thus one of the largest Global Warming Potentials among HFCs

167   (WMO, 2018). However, because it is not an ODS-substitute but an unintentional byprod-

168   uct of industrial HCFC-22 production, no future increase of HFC-23 is expected (Velders

169   et al., 2009). Therefore, it is not included in our analyses. The first setting is the ref-

170   erence ("control run"), for which all HFC abundances are set to 0. For the other exper-

171   iments, we assume different levels of continuous HFC production, thus different HFC con-

172   centrations in 2095. We initialize HFC amounts based on the radiative forcing simula-

173   tions of Velders et al. (2014), which use the upper and lower ranges of the HFC base-

174   line scenarios of Velders et al. (2009). Figure 4 of Velders et al. (2014) shows that, around

175   the end of the 21st century, radiative forcing due to unregulated HFCs (i.e., their im-

176   pact on the radiation budget in the troposphere) could become comparable to the in-

177   crease in CO_2 radiative forcing between 2000–2100 in the RCP2.6 scenario (Velders et

178   al., 2014).

179   Our purpose is to investigate the consequences for stratospheric O_3 in this case.

180   The lower and upper limits of the radiative forcing due to unregulated HFCs correspond,

181   respectively, to about twice and three times the radiative forcing in 2050 (Fig. 4 of Velders

182   et al., 2014). We call the former the "low-HFC" case and the latter the "high-HFC" case.

183   Assuming radiative forcing is proportional to the HFC amount, we set HFC surface mix-

184   ing ratios for the low- and high-HFC cases to, respectively, twice and three times the pro-

185   jected 2050 values of Hurwitz et al. (2015) (Table 1). Vertical HFC profiles are then cal-

186   culated in the CCMs by considering transport of HFCs and chemical loss from the re-

187   actions with $O(^1D)$, OH, and Cl.

188   Experiments are initialized using the output for 2095 from a sensitivity run of the

189   CCMI REF-C2 experiment (SEN-C2-RCP26, Morgenstern et al. (2018)). Calculations

190   continue for 110 years with ODS and GHG abundances fixed to their 2095 levels. For

191   SST and sea ice data, we use the monthly values of 10-year averages between 2090–2099.

192   Throughout a 110-year simulation, averages between 1960–2000 are used for the solar

193   irradiance seasonal cycle and SST/sea ice seasonal conditions for 2095 are repeated ev-

194   ery year. The first ten years are discarded from the analysis because they show transi-

195   tional changes from the initial state. We consider the last 100 years as a 100-member

196   ensemble. We focus on ensemble mean, yearly mean, zonally averaged results. We fur-

197   ther derive monthly averages for wave flux analysis.

3 Results

199   To evaluate the impact of HFCs on O_3 distribution in the stratosphere, we calcu-

200   late temperature, O_3, and residual circulation anomalies by comparing output from the

201   low- and high-HFC experiments with the control run for MIROC3.2-CCM and MIROC5-

202   CCM.

203   Unlike CO_2, which warms the troposphere and cools the stratosphere at all lati-

204   tudes, HFCs, like other halocarbons, consistently induce a latitude-dependent atmospheric

205   temperature increase, with a maximum around 100 hPa ($\sim$18 km) in the tropics (see Forster

206   & Joshi, 2005, for fixed dynamical heating simulations of temperature response to halo-

207   carbons and to CO_2 up to ∼5 hPa). This behaviour is well reproduced in the lower and

208   middle stratosphere by MIROC3.2-CCM (Figure 1, left) and MIROC5-CCM (Figure 1,

209   right) for the low-HFC (top row) and high-HFC (bottom row) cases. Horizontal and ver-

210   tical extension of the heating maximum matches the results of Forster and Joshi (2005)

211   in the low- and mid-latitude lower stratosphere (100–50 hPa for both models). Further-

212   more, temperature anomalies below ∼20 hPa are consistent with the 2D-model results

213   of Hurwitz et al. (2015). They also appear proportional to the HFC amount, as shown

214   by comparing the low-HFC and high-HFC cases.

215   In terms of ozone response, both models exhibit strong differences between low/mid-

216   latitudes and higher latitudes, especially in the Northern Hemisphere (NH) stratosphere

217   (Figure 2). At NH high latitudes, MIROC3.2-CCM indicates large positive O_3 anoma-

218   lies in the lower and middle stratosphere (400–10 hPa, Figure 2, left), that correspond

219   to increased temperature (Figure 1, left) and wintertime downwelling in the polar strato-

220   sphere (Figure 3). MIROC5-CCM also shows increased O_3 in the NH polar stratosphere

221   in response to HFCs. However, anomaly values are smaller than for MIROC3.2-CCM

222   and the maximum is narrower vertically, extending between 200–70 hPa only (Figure 2).

223   At low and mid-latitudes for MIROC3.2-CCM, O_3 anomalies between 200–5 hPa are al-

224   ternately positive, negative and positive (Figure 2, left). This pattern is found in both

225   low- and high-HFC cases (Figure 2, top left and bottom left, respectively) and, like for

226   temperature, response appears proportional to the HFC increase. Largest negative anoma-

227   lies are found between 50 and 20 hPa just below the peak of O_3 volume mixing ratio (VMR,

228   Figure 4). A similar alternating pattern is visible in MIROC5-CCM results (Figure 2, right).

229   Largest negative O_3 anomalies for MIROC5-CCM are found at mid-latitudes, further

230   from the Equator than for MIROC3.2-CCM.

231   The low-latitude alternating pattern found for MIROC3.2-CCM in the O_3 anoma-

232   lies (200–20 hPa) corresponds well to HFC-induced changes of the zonal mean residual

233   vertical motion ($\bar{w}^*$, Andrews et al., 1987), while the positive anomaly between 20–5 hPa

234   is due to the negative temperature response (Figure 1). These results are generally con-

235   sistent with the results of Hurwitz et al. (2015). At low and mid-latitudes, residual ver-

236   tical motion anomalies for MIROC5-CCM resemble those of MIROC3.2-CCM above 100

237   hPa (Figure 3, right). However, they are less structured below 100 hPa, with marked dif-

238   ferences between the low-HFC and high-HFC cases (colors levels, Figure 3, top right and

239   bottom right, respectively). At NH high latitudes, MIROC3.2-CCM results show large,

240 consistent downward motion anomalies in both low-HFC and high-HFC cases. The en-
241 hanced downward motion is likely responsible for the large O_3 anomalies seen in Figure 2.
242 Large negative vertical motion anomalies are also found for MIROC5-CCM in the po-
243 lar upper stratosphere, except between 50–10 hPa (Figure 3, right) where a small, up-
244 ward motion anomaly is visible. This positive anomaly explains the smaller and narrower
245 O_3 response maximum in MIROC5-CCM.

246   Since total ozone amount is an important factor for UV radiation, we also exam-
247 ine the HFC-induced total column O_3 anomalies (Figure 5). For MIROC3.2-CCM, there
248 is no apparent change in the total ozone amounts at low latitudes (30°S–30°N), because
249 the negative and positive O_3 anomalies (Figure 2) cancel out. However, the strong O_3
250 increase at NH mid- and high-latitudes is also visible in the total ozone anomalies. Quan-
251 titatively, this represents up to 4.2 DU (about 1% of the total O_3 amount). Because of
252 the complex vertical structure of MIROC5-CCM O_3 anomalies, the distribution of to-
253 tal O_3 anomalies shows multiple structures depending on the latitude. Anomalies are
254 globally small and positive (net increase of total O_3) at all latitudes, with maxima in the
255 Arctic, tropical and Antarctic regions. The largest net total O_3 increase for MIROC5-
256 CCM is found at NH high latitudes (70–80°N), but it does not exceed 1.2 DU ($\sim$0.3%
257 of the total O_3 amount).

4 Discussion

259   The complex patterns observed in the low-latitude O_3 anomaly distributions for
260 both models (Figure 2) result from a combination of chemically-induced effects, caused
261 by temperature changes in the upper stratosphere (Figure 1), and circulation changes
262 in the middle and lower stratosphere, where O_3 variations are mostly transport-driven
263 (Figure 3). The induced circulation changes below 50 hPa: increased subtropical upwelling
264 and equatorial downwelling, are indicated by positive and negative $\bar{w}^*$ anomalies, respec-
265 tively. These changes weaken the tropospheric Hadley circulation and limit the amount
266 of O_3-poor air transported upwards, thus explaining the positive O_3 anomaly below 50
267 hPa. Above 50 hPa, a consistently increased vertical motion (positive $\bar{w}^*$ anomalies) in-
268 duces advection of O_3-poor air from below, which explains the large negative anomalies
269 at the 50–20 hPa level. Above 20 hPa, O_3 anomalies are quite small and mostly driven
270 by temperature changes. In the NH polar stratosphere, the strong O_3 enhancement ob-
271 served in the MIROC3.2-CCM output corresponds to downward motion anomalies caused

272 by increased planetary wave activity in the wintertime (Figure 3, left). In MIROC5-CCM,

273 weaker heating of the NH polar stratosphere (Figure 1, right) and limited downward mo-

274 tion enhancement by HFCs (Figure 3, right) explain the smaller and narrower high-latitude

275 O_3 anomaly maximum.

276 To assess the significance of the simulated structures, we performed a t-test anal-

277 ysis between the control run and the HFC experiments among the 100 ensemble mem-

278 bers. In MIROC3.2-CCM, the low-latitude pattern was statistically significant at the 95%

279 level in both HFC simulations (Figure 6, left). The NH polar enhancement was also sig-

280 nificant at the 95% level for the high-HFC case, but significance was smaller for the low-

281 HFC case (central shaded patch, Figure 6, top left). We conclude that the observed fea-

282 tures are globally robust for MIROC3.2-CCM. They indicate clear connections between

283 temperature anomalies, residual vertical motion anomalies, and the O_3 distribution.

284 Conversely, t-test results for MIROC5-CCM showed few regions with significance

285 larger than 90–95%. Therefore, we set a lower threshold for MIROC5-CCM (66.7%, Fig-

286 ure 6, right). This indicates that variability among the ensemble members is larger in

287 MIROC5-CCM than in MIROC2.3-CCM and implies that the low-latitude alternating

288 pattern, though also visible in MIROC5-CCM output, cannot be as easily explained by

289 temperature and residual vertical motion anomalies as for MIROC3.2-CCM. Overall, MIROC3.2-

290 CCM shows a clear connection between HFC-induced anomalies (temperature, residual

291 vertical motion) and variations of the stratospheric O_3 distribution. MIROC5-CCM ex-

292 periments also show consistent temperature and O_3 response at mid- and high latitudes,

293 but with larger variability among ensemble members. Therefore, interpretation of MIROC5-

294 CCM results is less straightforward than for MIROC3.2-CCM, especially in terms of con-

295 nections between O_3, temperature and circulation anomalies.

296 Our analysis further indicates that discrepancy between the models at NH high lat-

297 itudes is caused by marked differences in the anomalies (left panels in Figures 7–10) of

298 the wave flux and wave flux divergence (Andrews et al., 1987). In MIROC3.2-CCM, large

299 anomalies are visible in the NH polar upper stratosphere (above 10–20 hPa) through-

300 out winter, with particularly large positive values near the pole in February. In MIROC5-

301 CCM, anomalies are more extensive in latitude and pressure, with higher values than

302 in MIROC3.2-CCM. On the contrary, seasonal evolution of the wave flux and wave flux

303 divergence (right panels) is similar for MIROC3-CCM and MIROC5-CCM. For both mod-

els, wave flux structures are complex and difficult to analyze because anomalies induced by HFC increases are much smaller than the climatological wave flux and its divergence, and because anomalies are highly sensitive to changes in stratospheric temperature and wind distributions.

5 Conclusion

We investigated the impact of increasing atmospheric HFC concentrations on the distribution of ozone in the stratosphere. For this purpose, we devised a set of experiments with varying amounts of HFCs and performed multi-member ensemble simulations based on two CCMs, MIROC3.2-CCM and MIROC5-CCM, which use the same module for stratospheric chemistry but have differences in the modeling of physical processes.

Our 3D-model simulations showed responses of O_3 and temperature to increasing HFC levels, at low and mid-latitudes, qualitatively similar to previous 2D-model results (Hurwitz et al., 2015). The observed alternating anomaly pattern could reasonably be explained by competing effects of residual vertical motion anomalies in the lower and middle stratosphere and temperature anomalies in the upper stratosphere. On the contrary, there were large differences at high latitudes, notably in the NH polar region, not only between the 2D and 3D simulations but even between the 3D models themselves. We showed that these discrepancies are due to differences of wave activity during winter. Results for O_3 at high latitudes should, however, be analyzed with caution. Indeed, small differences in the wintertime evolution of wave activity can cause considerable differences of ozone response between the models, resulting in large model uncertainty.

Quantitatively, the estimated impact of HFCs on total ozone is small, at most 1% (4.2 DU) for MIROC3.2-CCM and 0.3% (1.2 DU) for MIROC5-CCM. In both cases, the net effect is positive. This differs from the 2D results of Hurwitz et al. (2015) who, adding total column anomalies at all latitudes, calculated a net global decrease of total O_3 of about 0.11 DU. Even with very favorable settings (continuous, unregulated emissions and RCP2.6 scenario for CO_2), our study shows that the impact of increasing HFC amounts on stratospheric O_3 at the end of the century will likely be very limited.

Acknowledgments

References

Akiyoshi, H., Nakamura, T., Miyasaka, T., Shiotani, M., & Suzuki, M. (2016). A nudged chemistry-climate model simulation of chemical constituent distribution at northern high-latitudes observed by SMILES and MLS during the 2009/2010 stratospheric sudden warming. *J. Geophys. Res. Atm.*, *121*, 1361–1380. doi: 10.1002/2015JD023334

Amos, M., Young, P. J., Hosking, J. S., Lamarque, J.-F., Garcia, R. R., Abraham, N. L., . . . Yamashita, Y. (2020). Projecting ozone hole recovery using an ensemble of chemistry-climate models weighted by model performance and independence. *Atmos. Chem. Phys.*, *20*, 9961–9977. doi: 10.5194/acp-20-9961-2018

Andrews, D. G., Holton, J. R., & Leovy, C. B. (1987). *Middle atmosphere dynamics.* New York, USA: Elsevier Science. (Issue 40 of International Geophysics Series,

364   ISSN 0074-6142, 489 pp.)

365 Bednarz, E. M., Maycock, A. C., Abraham, N. L., Braesicke, P., Dessens, O., &

366   Pyle, J. A.   (2016).   Furture Arctic ozone recovery: the importance of

367   chemistry and dynamics.   *Atmos. Chem. Phys.*, *16*, 12159–12176.   doi:

368   10.5194/acp-16-12159-12176

369 Bernath, P. F., McElroy, C. T., Abrams, M. C., Boone, C. D., Butler, M., Camy-

370   Peyret, C., . . . Zou, J.   (2005).   Atmospheric Chemistry Experiment

371   (ACE): Mission overview.   *Geophys. Res. Lett.*, *32*(15), L15S01.   doi:

372   10.1029/2005GL022386

373 Dhomse, S. S., Kinnison, D., Chipperfield, M. P., Salawitch, R. J., Cionni, I.,

374   Hegglin, M. I., . . . Zeng, G.   (2018).   Estimates of ozone return dates from

375   Chemistry-Climate Model Initiative simulations.   *Atmos. Chem. Phys.*, *18*(11),

376   8409–8438. doi: 10.5194/acp-18-8409-2018

377 Fernando, A. M., Bernath, P. F., & Boone, C. D.   (2019).   Trends in atmospheric

378   HFC-23 (CHF$_3$) and HFC-134a abundances.   *J. Quant. Spectrosc. Radiat.*

379   *Transfer*, *238*, 106540. doi: 10.1016/j.jqsrt.2019.06.019

380 Forster, P. M., & Joshi, M. (2005). The role of halocarbons in the climate change of

381   the troposphere and stratosphere.   *Clim. Change*, *71*, 249–266.   doi: 10.1007/

382   s10584-005-5955-7

383 Hurwitz, M., Fleming, E. L., Newman, P. A., Li, F., Mlauer, E., Cady-Pereira, K.,

384   & Bailey, R.   (2015).   Ozone depletion by hydrofluorocarbons.   *Geophys. Res.*

385   *Lett.*, *42*, 8686–8692. doi: 10.1002/2015GL065856

386 IPCC.   (2014).   *Climate Change 2014: Synthesis Report. Contribution of Working*

387   *Groups I, II and III to the Fifth Assessment Report of the Intergovernmen-*

388   *tal Panel on Climate Change* [Core Writing Team, R. K. Pachauri and L. A.

389   Meyer (eds.)]. IPCC, Geneva, Switzerland, 151 pp.

390 K1 model developers.   (2004).   *K-1 coupled GCM (MIROC) description* (K-1 Tech.

391   Rep., 34 pp.)   Edited by H. Hasumi and S. Emori, Center for Climate System

392   Research (CCSR), University of Tokyo; National Institute for Environmental

393   Studies (NIES), Frontier Research Center for Global Change (FRCGC).

394 Lunt, M. F., Rigby, M., Ganesan, A. L., Manning, A. J., Prinn, R. G., O'Doherty,

395   S., . . . Simmonds, P. G.   (2015).   Reconciling reported and unreported HFC

396   emissions with atmospheric observations.   *Proc. Natl. Acad. Sci.*, *111*(19),

5927–5931. doi: 10.1073/pnas.1420247112

Montzka, S. A., Dutton, G. S., Yu, P., Ray, E., Portmann, R. W., Daniel, J. S., . . . Elkins, J. W. (2018). An unexpected and persistent increase in global emissions of ozone-depleting CFC-11. *Nature*, *557*, 413-417. doi: 10.1038/s41586-018-0106-2

Montzka, S. A., McFarland, M., Andersen, S. O., Miller, B. R., Fahey, D. W., Hall, B. D., . . . Elkins, J. W. (2015). Recent Trends in Global Emissions of Hydrochlorofluorocarbons and Hydrofluorocarbons: Reflecting on the 2007 Adjustments to the Montreal Protocol. *J. Phys. Chem.*, *119*(19), 4439–4449. doi: 10.1021/jp5097376

Morgenstern, O., Hegglin, M. I., Rozanov, E., O'Connor, F. M., Abraham, N. L., Akiyoshi, H., . . . Zeng, G. (2017). Review of the global models used within phase 1 of the Chemistry–Climate Model Initiative (CCMI). *Geosci. Model Dev.*, *10*, 639–671. doi: 10.5194/gmd-10-639-2017

Morgenstern, O., Stone, K. A., Schofield, R., Akiyoshi, H., Yamashita, Y., Kinnison, D. E., . . . Chipperfield, M. P. (2018). Ozone sensitivity to varying greenhouse gases and ozone-depleting substances in CCMI-1 simulations. *Atmos. Chem. Phys.*, *18*(2), 1091–1114. doi: 10.5194/acp-18-1091-2018

Nassar, R., Bernath, P. F., Boone, C. D., McLeod, S. D., Skelton, R., Walker, K. A., . . . Duchatelet, P. (2006). A global inventory of stratospheric fluorine in 2004 based on Atmospheric] Chemistry Experiment Fourier transform spectrometer (ACE-FTS) measurements. *J. Geophys. Res.*, *11*, D22313. doi: 10.1029/2006JD007395

Numaguti, A., Takahashi, M., Nakajima, T., & Sumi, A. (1997). *Description of CCSR/NIES Atmospheric General Circulation Model.* CGER's Supercomputer Monograph Report, Center for Global Environmental Research, National Institute for Environmental Studies, No. 3, pp. 1–48.

Simmonds, P. G., Rigby, M., McCulloch, A., O'Doherty, S., Young, D., Mühle, J., . . . Prinn, R. G. (2017). Changing trends and emissions of hydrochlorofluorocarbons (HCFCs) and their hydrofluorocarbon (HFCs) replacements. *Atmos. Chem. Phys.*, *17*(7), 4641–4655. doi: 10.5194/acp-17-4641-2017

SPARC. (2013). *SPARC Report on the Lifetimes of Stratospheric Ozone-Depleting Substances, Their Replacement, and Related Species* [M. Ko, P. Newman, S.

Reimann, S. Strahan (Eds.)]. SPARC Report No. 6, WRCP-15/2013.

Stanley, K. M., Say, D., Mühle, J., Harth, C. M., Krummel, P. B., Young, D., . . . Rigby, M. (2020). Increase in global emissions of HFC-23 despite near-total expected reductions. *Nat. Comm.*, *11*, 397. doi: 10.1038/s41467-019-13899-4

UNEP. (2011). *HFCs: A Critical Link in Protecting Climate and the Ozone Layer.* United Nations Environment Programme (UNEP), 36pp.

Velders, G. J. M., Fahey, D. W., Daniel, J. S., McFarland, M., & Andersen, S. O. (2009). The large contribution of projected HFC emissions to future climate forcing. *Proc. Natl. Acad. Sci.*, *106*(27), 10949–10954. doi: 10.1073/pnas.0902817106

Velders, G. J. M., Solomon, S., & Daniel, J. S. (2014). Growth of climate change commitments from HFC banks and emissions. *Atmos. Chem. Phys.*, *14*, 4563–4572. doi: 10.5194/acp-14-4563-2014

Watanabe, M., Suzuki, T., O'ishi, R., Komuro, Y., Watanabe, S., Emori, S., . . . Kimoto, M. (2010). Improved Climate Simulation by MIROC5: Mean States, Variability, and Climate Sensitivity. *J. Climate*, *23*(23), 6312–6335. doi: 10.1175/2010JCLI3679.1

WMO. (2014). *Scientific Assessment of Ozone Depletion: 2014.* World Meteorological Organization (WMO), Global Ozone Research and Monitoring Project–Report No. 55, 416 pp., Geneva, Switzerland.

WMO. (2018). *Scientific Assessment of Ozone Depletion: 2018.* World Meteorological Organization (WMO), Global Ozone Research and Monitoring Project–Report No. 58, 588 pp., Geneva, Switzerland.

Table 1. Initial abundance settings for the four HFC species considered in the simulations[a].

|	HFC-125	HFC-143a	HFC-32	HFC-134a
Control run	—	—	—	—
Low-HFC case[b]	1.60 ppbv	1.10 ppbv	0.84 ppbv	0.64 ppbv
High-HFC case[c]	2.40 ppbv	1.65 ppbv	1.26 ppbv	0.96 ppbv

[a]assuming unmitigated production until the end of the century.

[b]twice the 2050 surface abundance of Hurwitz et al. (2015).

[c]three times the 2050 surface abundance of Hurwitz et al. (2015).
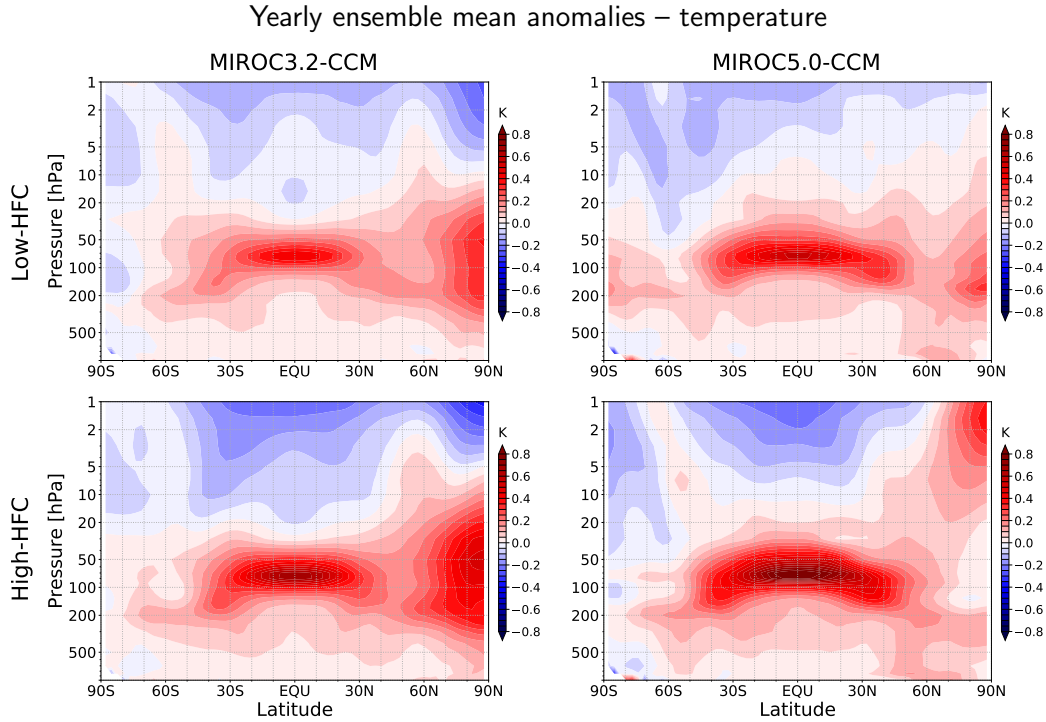
Figure 1. Zonal averages of ensemble mean, yearly mean temperature anomalies for MIROC3.2-CCM (left) and MIROC5-CCM (right). Anomalies (differences from the control run) are shown for the low-HFC (top) and high-HFC (bottom) cases. Red and blue color levels indicate heating (positive HFC-induced anomalies) and cooling (temperatures lower than the control run), respectively.
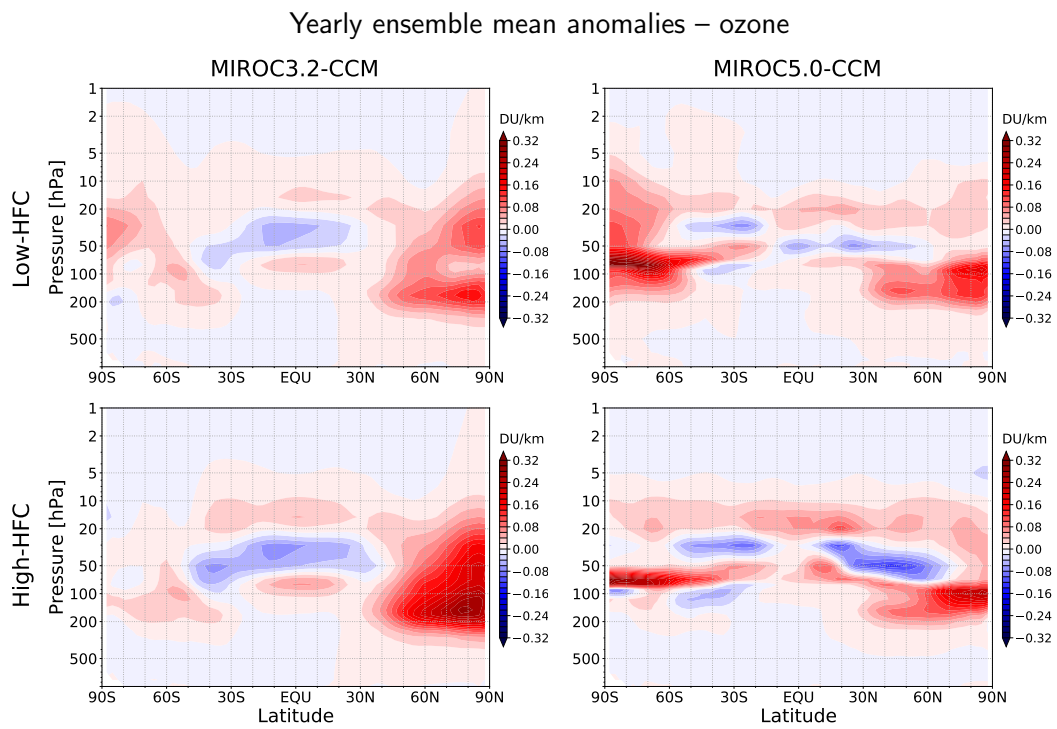
**Figure 2.** Same as Figure 1, but for O_3 partial column anomalies.
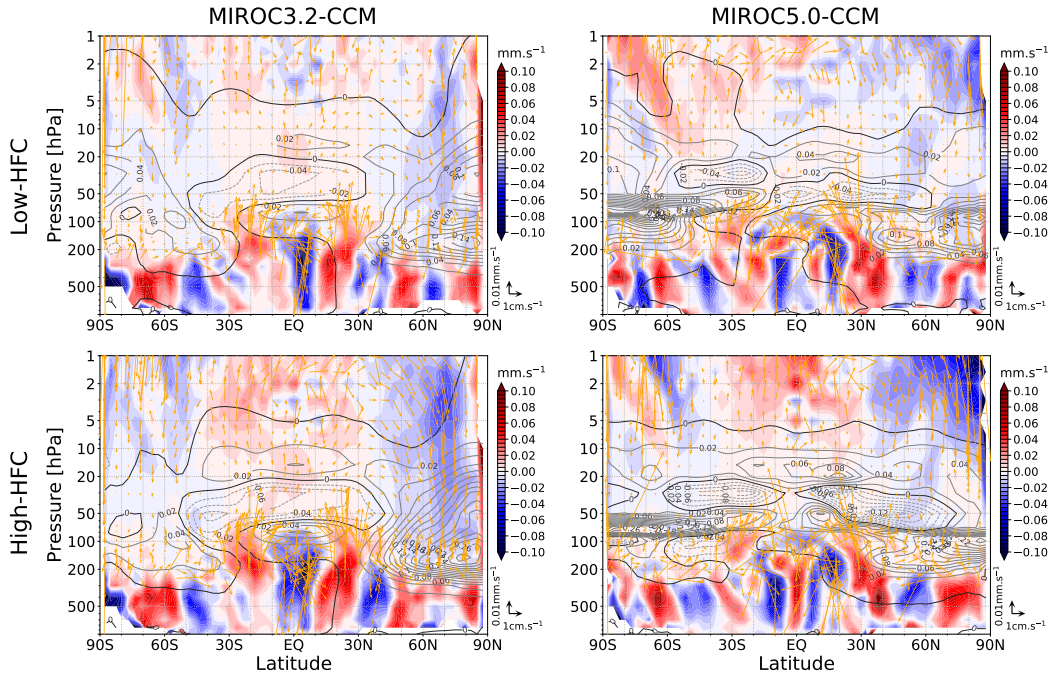
Figure 3. Vertical anomalies of the residual mean circulation (w* anomalies in mm.s^{-1}, color levels) and residual mean circulation changes (yellow arrows). Meridional (v*) and vertical (w*) circulation arrow components are scaled for visibility (see key). O$_3$ anomalies from Figure 2 are shown by the line contours. Layout is the same as in Figure 1.
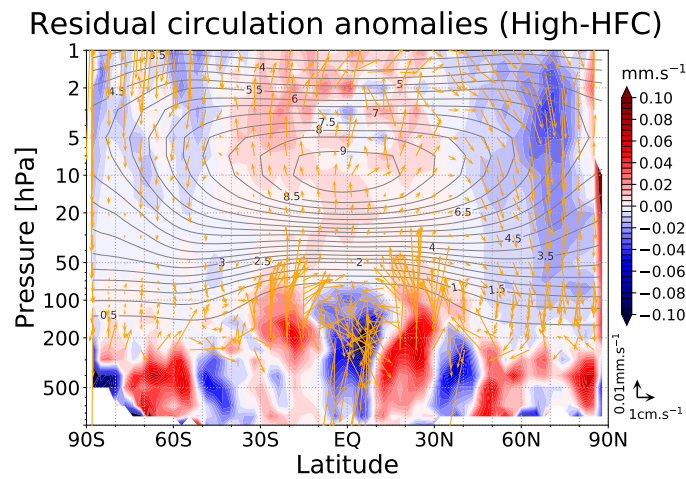

Figure 4. Same as Figure 3 in the high-HFC case for MIROC3.2-CCM, but with line contours showing the O$_3$ volume mixing ratio from the control run in parts-per-million-in-volume (0.5 ppmv spacing).
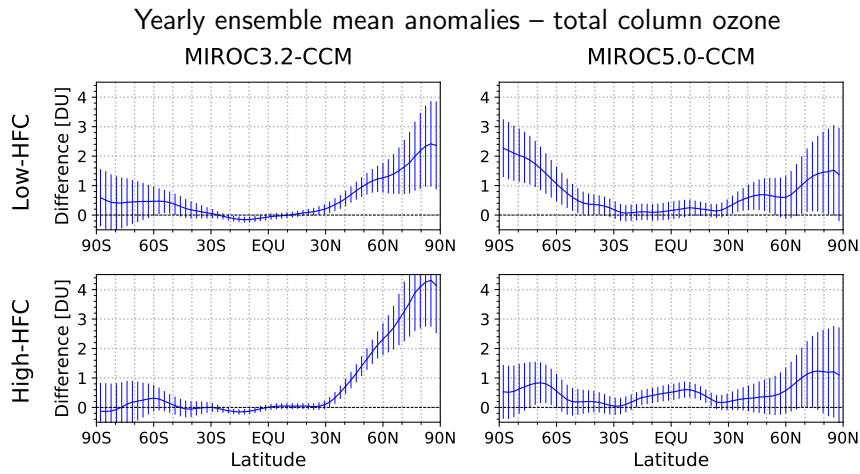
Figure 5. Zonally averaged ensemble mean, yearly mean total column O_3 anomalies for MIROC3.2-CCM (left) and MIROC5-CCM (right) in the low-HFC (top) and high-HFC (bottom) cases. Latitude range and grid point spacing are the same as in Figure 1. Total column is calculated over the full model vertical range (surface to ~0.003 hPa). Error bars represent the ensemble mean standard deviation.
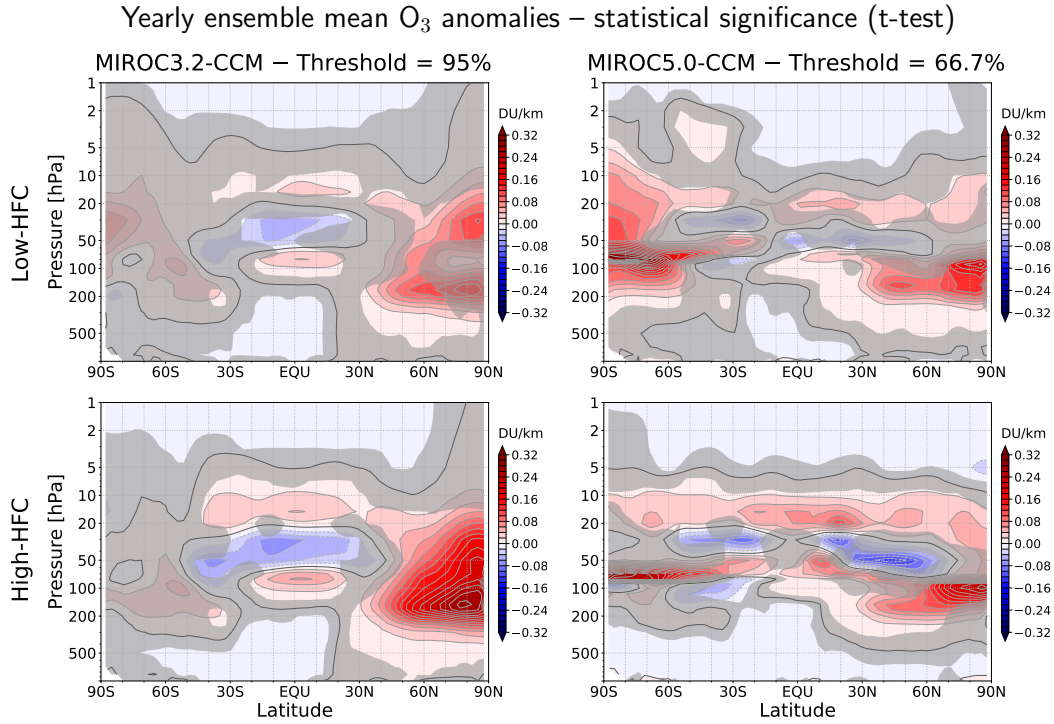
Figure 6. Same as Figure 2, but with statistical evaluation of anomaly structures. Shading shows low statistical significance areas, with thresholds of 95% for MIROC3.2-CCM (left) and ~67% for MIROC5-CCM (right). Unmasked regions are above the significance threshold. The thick black line (0 DU/km) shows the transition region between positive and negative anomalies, where calculated significance was lowest.
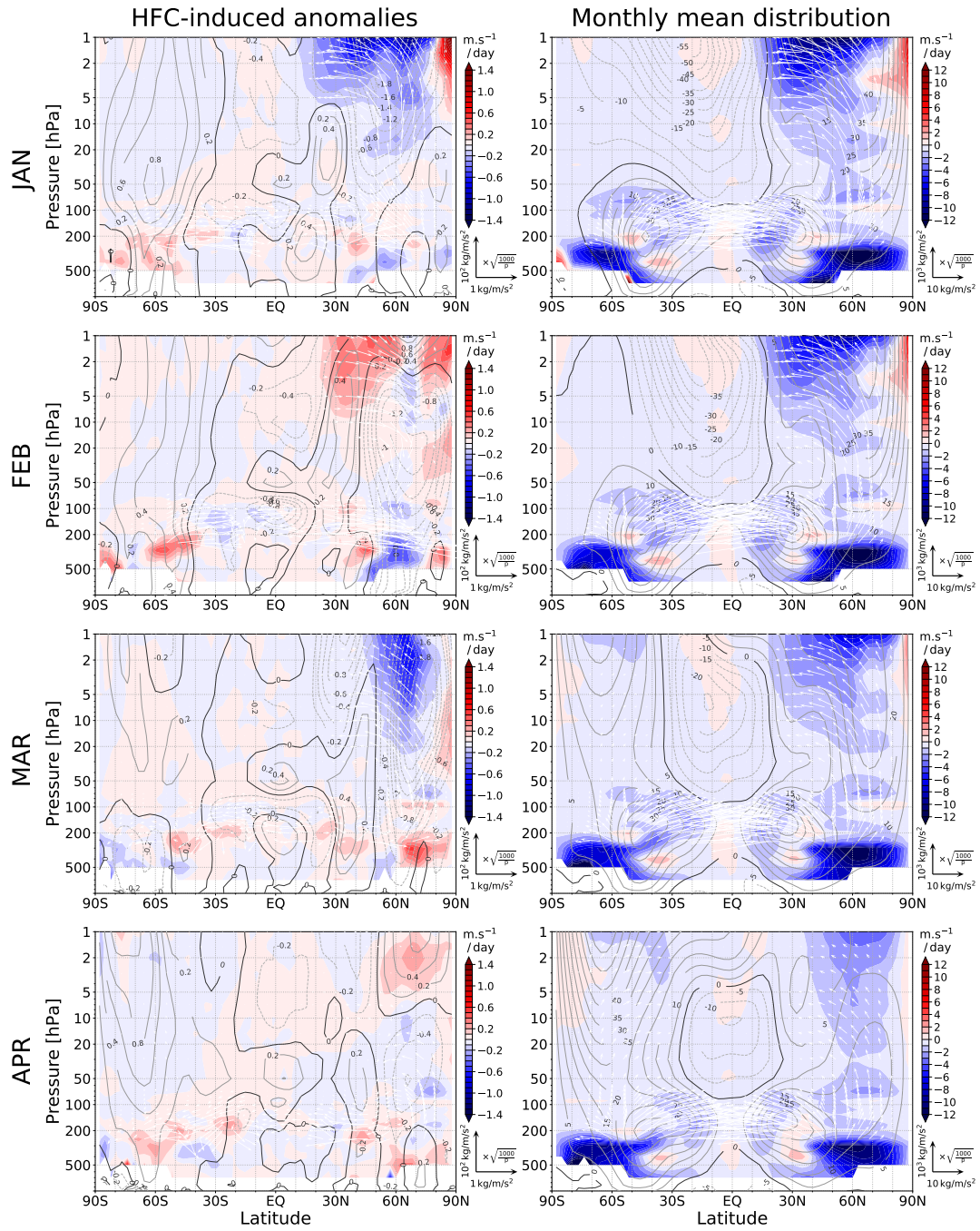
Figure 7. Eliassen-Palm (EP) flux, EP flux divergence and zonal mean zonal wind for MIROC3.2-CCM in the low-HFC case. *Left*: Monthly mean anomalies from January (top) to April (bottom). Color levels show positive (red) and negative (blue) anomalies of the EP flux divergence. Positive and negative zonal mean zonal wind anomalies are shown by the solid and dashed lines, respectively. White arrows represent EP flux anomalies (see key on the right hand side), with a pressure-dependent scaling (also indicated) to enhance visibility of the stratospheric vectors. *Right*: Same as left column, but for monthly mean distributions.
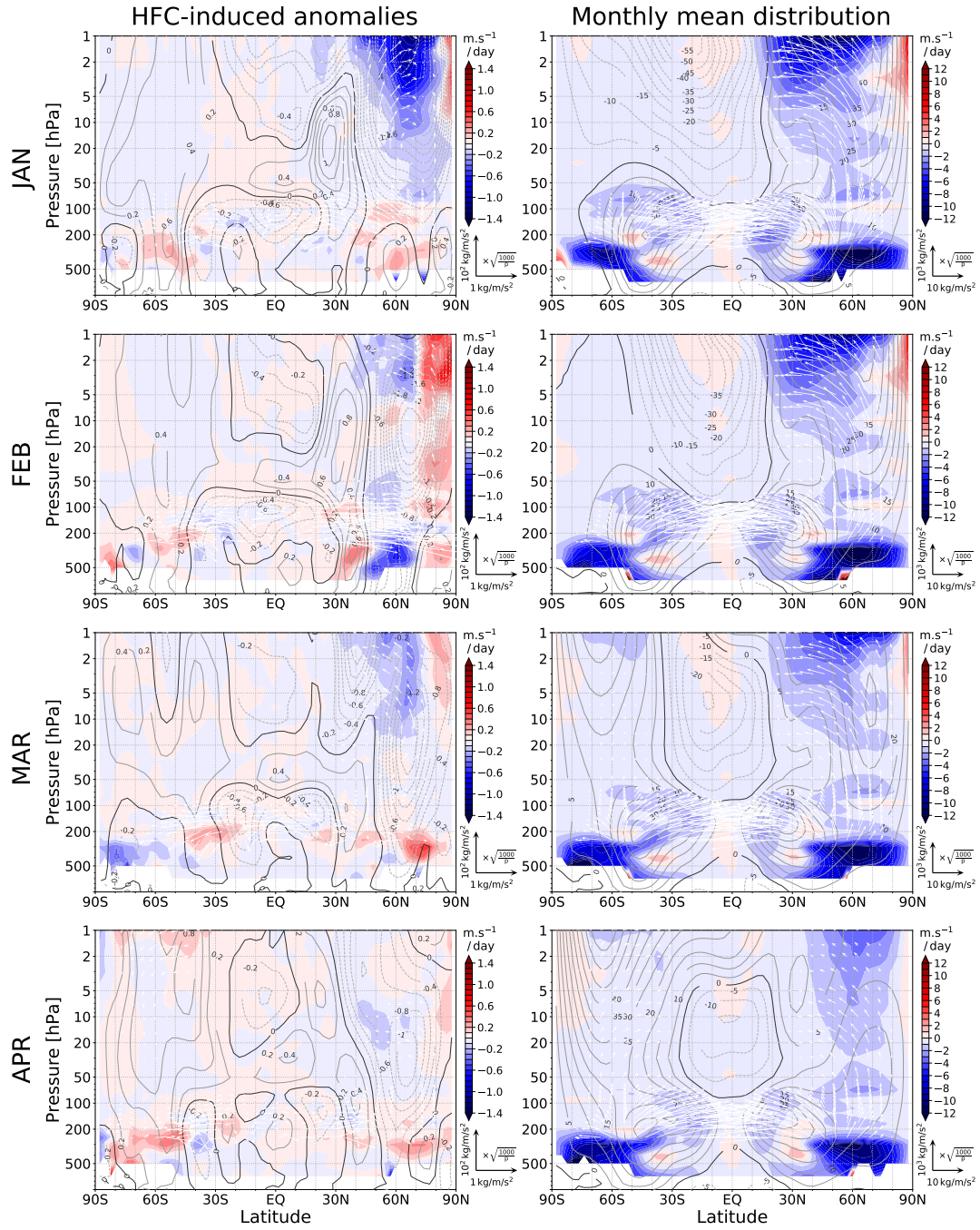
Figure 8. Same as Figure 7, but for MIROC3.2-CCM in the high-HFC case.
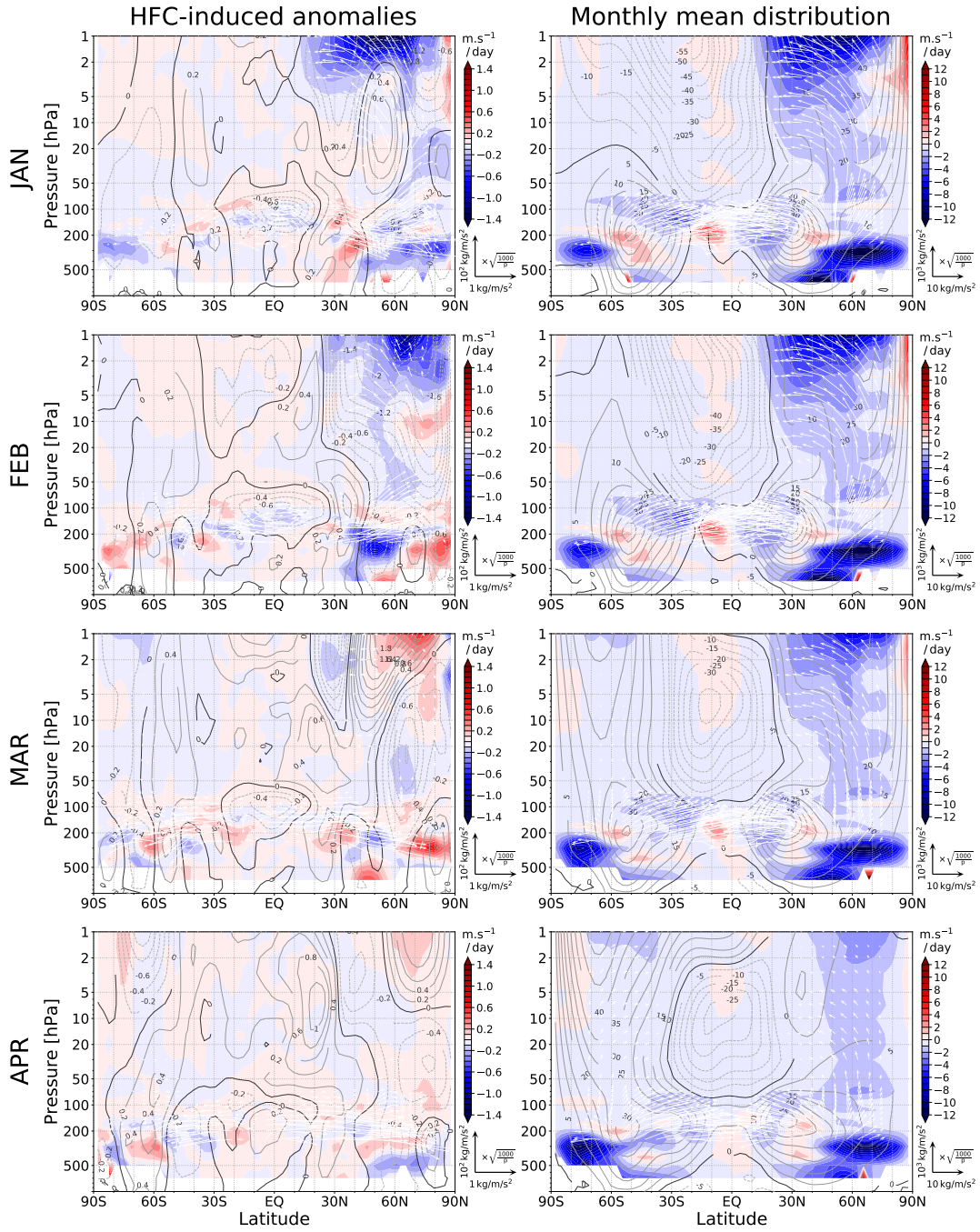
Figure 9. Same as Figure 7, but for MIROC5-CCM in the low-HFC case.
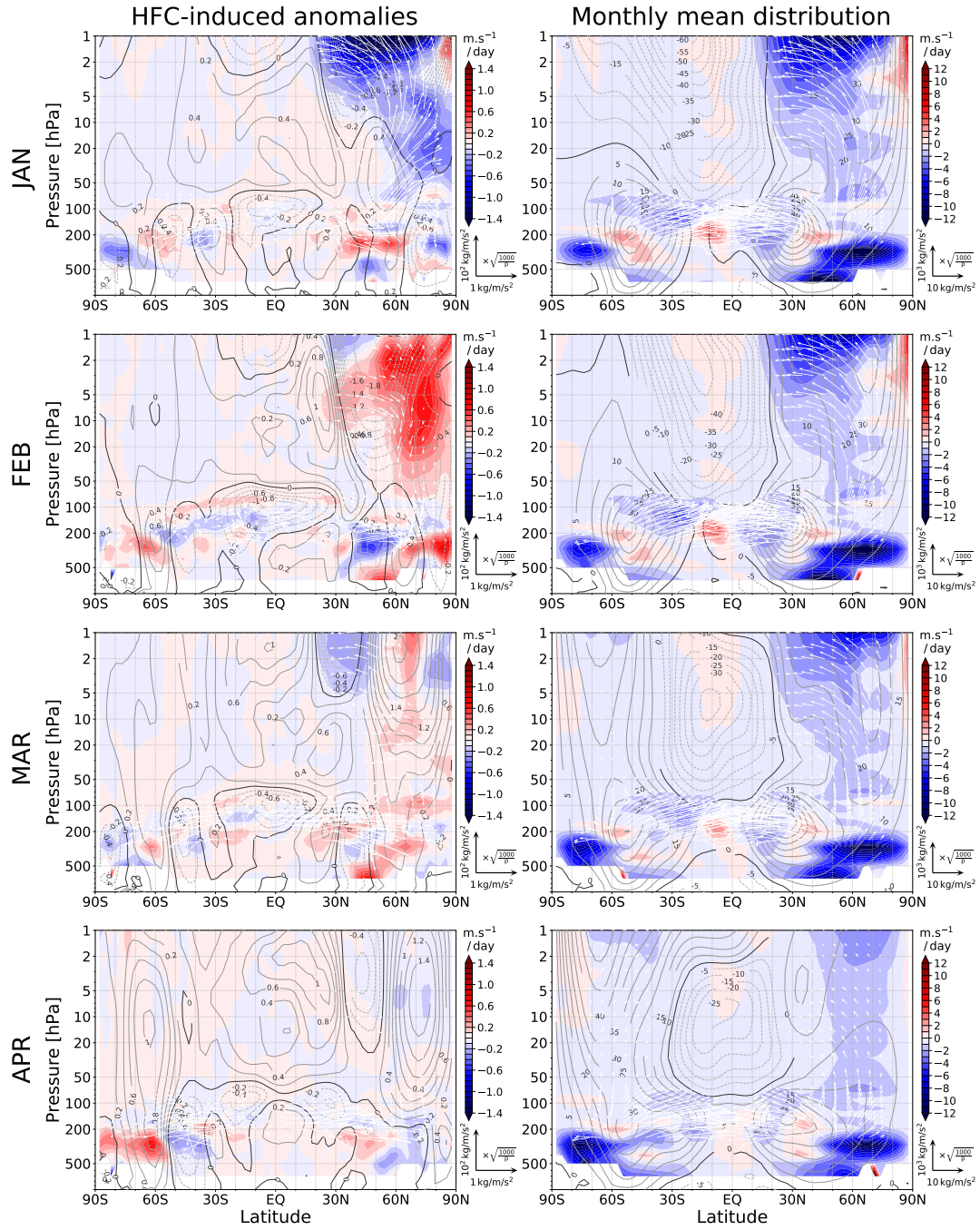
Figure 10. Same as Figure 7, but for MIROC5-CCM in the high-HFC case.